

# STUDY OF TIP-CLEARANCE FLOW IN TURBOMACHINES USING LARGE-EDDY SIMULATION

*A powerful computational technique, large-eddy simulation, helps researchers study the detailed flow dynamics in the tip-gap region of hydraulic turbomachines. LES also helps researchers investigate ways to mitigate undesirable effects, such as cavitation, which can lead to reduced performance, increased noise, and structural vibration and erosion.*

In hydraulic turbomachines, such as submarine propulsors and liquid fuel pumps, a small radial gap between a rotor-blade tip and casing wall is unavoidable. This tip gap, also known as tip clearance, is a major source of cavitation, which results in spontaneously formed bubbles. This in turn can result in loud noise, structural vibration, performance deterioration, and erosion of the blade and the casing wall.<sup>1,2</sup> These unfavorable effects have motivated theoretical, experimental, and numerical studies since the 1950s.

Although researchers generally recognize that cavitation is associated with low-pressure events generated by vortical and turbulent fluid motions around and downstream of the tip gap, they do not yet fully understand the underlying mechanisms. This is primarily due to limitations of conventional approaches in providing data on the detailed unsteady fluid dynamics and the resulting cavitation-inducing low-pressure events. Because

a tip-clearance flow's important features develop near the casing wall, where blades rotate at a high speed, experimental measurements are difficult and often dangerous. It's also impractical to measure both the unsteady velocity and pressure over a large spatial region. In computational studies, researchers have traditionally relied on the Reynolds-averaged Navier-Stokes (RANS) equations in conjunction with a turbulence model. In such an approach, they only explicitly compute the time-averaged (or ensemble-averaged) flow-field and model the effect of the time-dependent motion of all flow scales.

To gain insight into the mechanisms of tip-leakage cavitation, we need to study the detailed vortex and turbulence dynamics in the rotor-blade wake and the tip-clearance region. This understanding is also a necessary precursor to devising efficient cavitation-control methodologies. To this end, we can employ the modern turbulence-simulation technique of *large-eddy simulation* (LES). Unlike RANS, LES explicitly computes a range of energetic flow scales, and it only models the flow scales smaller than the computational cell size. These models are called *subgrid-scale* (SGS) models. Because of its ability to resolve the energy-containing fluid motions temporally and spatially as well as provide both the time-varying velocity and pressure, LES is well-suited for studying the tip-leakage flow.

1521-9615/04/\$20.00 © 2004 IEEE  
Copublished by the IEEE CS and the AIP

DONGHYUN YOU, MENG WANG, AND PARVIZ MOIN

Stanford University

RAJAT MITTAL

George Washington University

## Flow Configuration and Computational Challenges

To validate the LES results, we chose the flow investigated experimentally by William Devenport's research group at Virginia Tech.<sup>3</sup> The experiment somewhat simplifies the flow configuration: instead of rotating blades, they considered a linear cascade (see Figure 1). They emulated the relative motion between the blade tips and casing wall using a moving belt underneath the tip gap. This flow configuration captures the essential physics despite its relative simplicity.

Devenport's experiment uses the following important parameters: The Reynolds number is 400,000, based on the blade chord ( $C$ ) and free-stream velocity of the inflow. The inlet turbulent boundary layer has a Reynolds number of 780 based on the momentum thickness. The blade pitch is  $0.9C$ , and the blade span is  $1C$ . The blade has a relatively high stagger angle of about 57 degrees. The size of the baseline tip gap is  $0.0165C$ ; two additional tip gaps, of sizes one-half and twice the baseline value, are considered as well.

An accurate LES of this flow is challenging due to the large mesh-size requirement, the simulation's 3D nature, and the need for statistical convergence and long-time sampling. To reduce the computational cost and problem size to a manageable level, we considered a single blade passage, with periodic boundary conditions in the pitch-wise ( $y$ ) direction to mimic the flow in multiblade passages. Figure 1 schematically shows the computational domain and coordinate definitions. The computational domain is  $1.8C \times 0.929C \times 0.5C$ , in the  $x$ ,  $y$ , and  $z$  directions, respectively. We used between 20 and 25 million grid points, and each simulation required  $O(10^3)$  single-processor CPU hours on an SGI Origin 3800, about 10 Gbytes of memory, and more than 1 Tbyte of disk space.

## Numerical Method

The fundamental equations governing fluid motion are the Navier-Stokes (momentum) equations and the equation for mass conservation. In our LES, we solve the spatially filtered, 3D, unsteady, and incompressible Navier-Stokes equations in conjunction with a Lagrangian dynamic SGS model,<sup>4</sup> which provides the SGS stresses required to close the equations. We discretized spatial derivative terms in the governing equations using second-order central differences. Time integration is based on a fully implicit fractional step method, which consists of two iterative schemes. We used the first one to solve the momentum equations and the second to solve the discretized Poisson equation for pressure, which

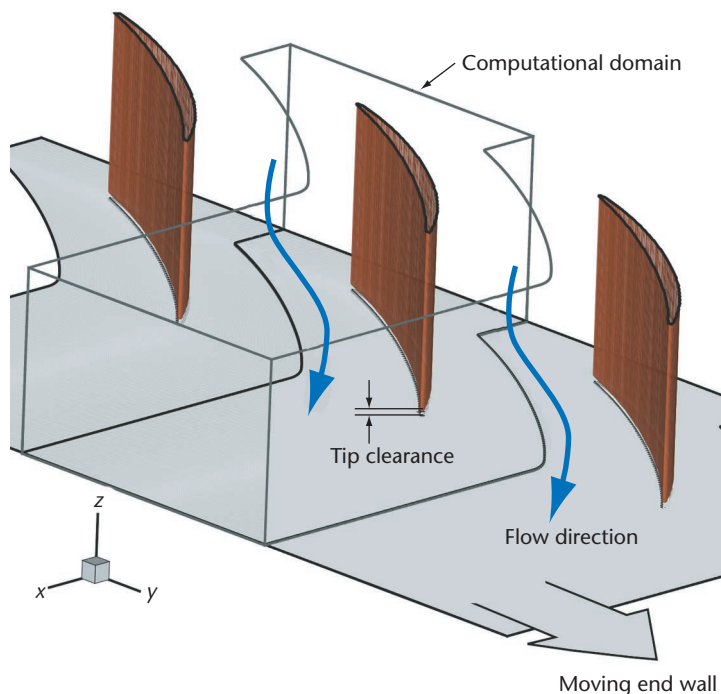
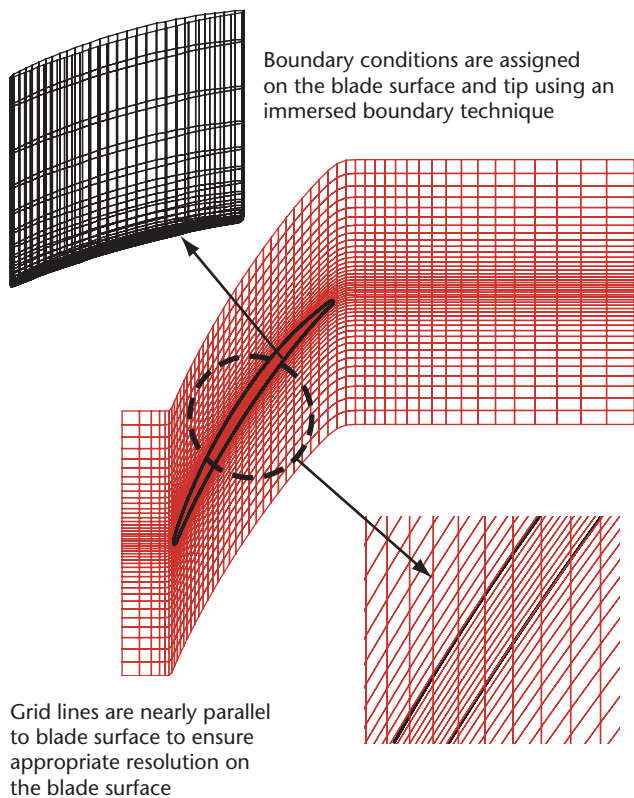


Figure 1. Flow configuration and coordinate system for large-eddy simulation of tip-clearance flow in a linear cascade with a moving end wall.

is required to enforce mass conservation. The same Poisson equation is widely used in other scientific and engineering disciplines, and hence, its solution and parallelization methods discussed here are of interest beyond fluid mechanics. These iterative routines take most of the CPU time, and therefore, it's crucial to improve both the numerical algorithms and parallel performance.

The tip-gap region imposes a geometric challenge for grid generation and computation of the flow. Previously used grid topologies, typically developed for RANS calculations, are unsuitable for LES because of the high stretching and aspect ratios of the grid cells. We eliminated this difficulty by using a novel approach that combines an immersed boundary technique with a curvilinear structured grid. The immersed boundary technique lets boundary conditions be imposed on a simple, non-body-conforming grid through a body force term in the momentum equations.<sup>5</sup> In the present study, we combine the immersed boundary method with a nearly body-conforming grid instead of the commonly used Cartesian grid. Using this approach, we can allocate sufficient resolution near the blade surface and within the tip gap, maintain high grid quality, and at the same time, effectively impose boundary conditions on the blade surface (see Figure 2).



**Figure 2.** Grid topology used to compute tip-clearance flow. A combination of structured curvilinear mesh with an immersed boundary method allows simplified grid topology in the tip-gap region while maintaining high mesh quality and resolution.

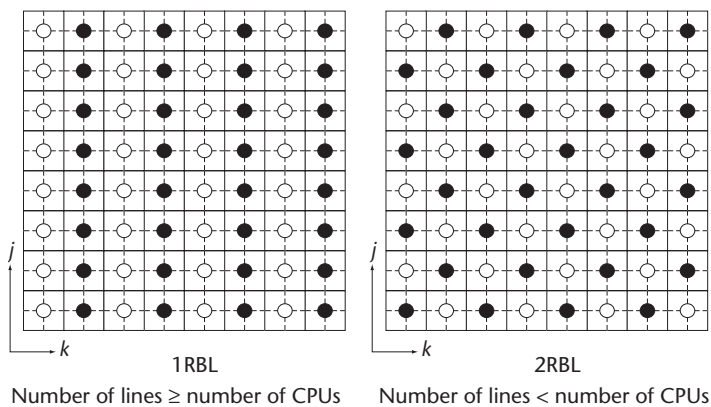


**Figure 3.** Illustration of the parallel implementation of multigrid method. A tridiagonal solver is employed along the  $j$ -direction.

### Parallelization for Shared-Memory Platforms

The introduction of faster shared-memory and shared-distributed-memory machines at the High-Performance Computing Modernization Program

(HPCMP) Major Shared Resource Centers (MSRC) has motivated us to parallelize our simulation code using OpenMP and enhance its portability. Since OpenMP lets us parallelize a serial code by inserting predefined parallelization directives, usually the implementation is easier than MPI parallelization. Also, data distribution issues never arise in the shared-memory implementation. However, the OpenMP implementation's parallel performance observed in the literature shows rapid saturation as the number of CPUs increases. Except for system-based issues such as nonuniform memory access and the finite bandwidth of a common bus of certain systems, the lack of strategies for shared-memory parallelization is a main cause for the parallel performance degradation. Considering that efficient memory use is the key factor for parallel speedup in the OpenMP parallelization, we made significant effort to design algorithms retaining memory efficiency. The code is currently compatible with the SGI Origin series, Compaq GS/ES series, Sun Enterprise series, and IBM Regatta P4 without source-level modifications.

The computation of momentum equations starts with computing the SGS eddy viscosity, used to model the stresses arising from SGS motion. However, the dynamic procedure for this computation involves numerical operations such as filtering and averaging of flow quantities, which increase the stack memory requirement considerably in the standard shared-memory approach. To overcome this difficulty, we decompose the computational domain by the number of CPUs available (as often used in distributed-memory parallelization). We use two or three overlapped mesh points between neighboring domains to handle data dependency during the computation. Once the contribution of SGS motions is obtained, the momentum equations, discretized into a set of algebraic equations, are solved iteratively.

The Poisson solver, based on a multigrid algorithm, is the most expensive part of the LES code. We have performed extensive studies to improve both the convergence and parallel efficiency for large-scale computations. Multigrid methods have been popular for this purpose, but using multigrids in all three dimensions requires memory several times larger than the amount needed for a base grid, and it complicates the coarsening procedure. On the contrary, 2D multigrid coarsening with a direct solution procedure in the remaining direction requires much less memory and is easier to optimize. Both the line Gauss-Seidel and red-black Gauss-Seidel methods<sup>6</sup> have attractive features for the latter strategy, and they have also shown good convergence properties and parallelizability in various applications.

We have considered two possible combinations

of the line and red-black Gauss-Seidel methods. The first approach consists of a 1D red-black (even-odd) method and the line Gauss-Seidel method (1RBL). The second approach consists of 2D red-black ordering and a tridiagonal matrix solver along the remaining dimension (2RBL).

With the same coarsening strategy and restriction (as well as prolongation) levels, we obtained similar convergence trends for both combinations. Test simulations show that the second approach has slightly better convergence properties, whereas the first approach gives better parallel speedup. We observed fast performance saturation in 2RBL due to reduced data locality and the resulting increase in cache miss, whereas in 1RBL, the maximum number of utilizable CPUs is limited by the number of lines at the highest multilevel. However, we can remedy these disadvantages by combining the two methods. This results in a technique with better parallel speedup at a larger number of CPUs as well as faster convergence.

Considering that 1RBL is better than 2RBL in the parallel performance, we first apply the 1RBL up to the multilevel where all CPUs can be used and then switch to 2RBL when the number of grid lines is smaller than the number of CPUs requested. Figure 3 illustrates this method. This combination is also advantageous because 2RBL shows a good convergence property on a coarser mesh.

We have evaluated the code's parallel performance on three different shared-memory computer systems: SGI Origin 3800, IBM Regatta P4, and Compaq GS320. Figure 4 gives the results. Considering that most of the recent shared- and shared-distributed-memory systems are based on a nonuniform memory access (NUMA) architecture, we have made an effort to retain data locality and low cache contention. Deviation from linear speedup is more significant on the Compaq GS320, which has the smallest memory capacity among the tested platforms. The actual speedups obtained on SGI Origin 3800 and IBM Regatta P4 platforms are close to the linear speedup. In general, difficulty in constructing optimal loops for momentum equations and the increase in cache miss due to the huge memory requirement in the Poisson solver are two major factors responsible for parallel speedup degradation.

### Tip-Leakage Flow Analysis

The large quantities of simulation data, which contain the space-time histories of the velocity and pressure fields, help us track the evolution of instantaneous flow features and perform the statistical analysis required to extract useful information about the physical mechanisms leading to cavitation.

The flowfield in the vicinity of the tip gap is

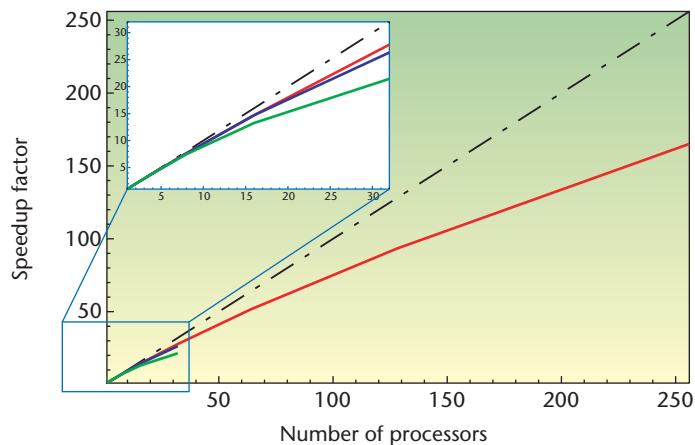


Figure 4. Parallel speedup achieved on various platforms. The red line shows the SGI Origin 3800; blue line, IBM Regatta P4; green line, Compaq GS320; and black line, linear speedup.

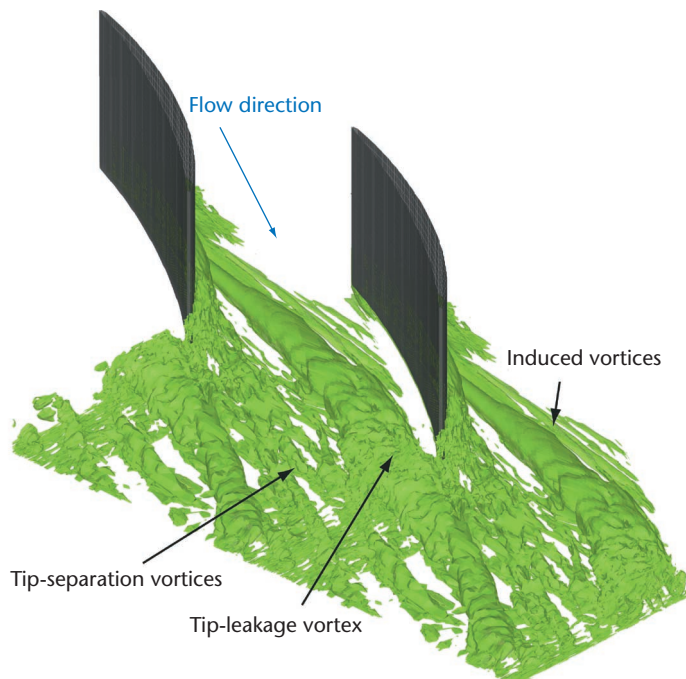


Figure 5. Vortical structures found in the tip-clearance flow as visualized by a vortex identification method.<sup>7</sup>

characterized by complex vortex structures and their interaction with the end-wall turbulent boundary layer and the blade wake. Figure 5 shows typical vortical structures predicted by the LES as visualized using Jinhee Jeong and Fazole Hussain's vortex identification method.<sup>7</sup>

The dominant vortical structure is the tip-leakage vortex generated near the blade's leading edge; it convects downstream while expanding in size.

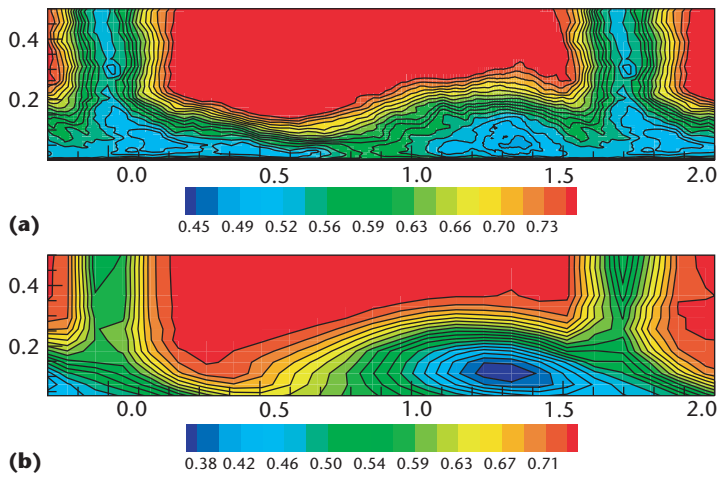


Figure 6. Mean stream-wise velocity contours in a  $y$ - $z$  plane roughly half-chord downstream from the trailing edge. (a) Present large-eddy simulation and (b) experiment.<sup>3</sup>

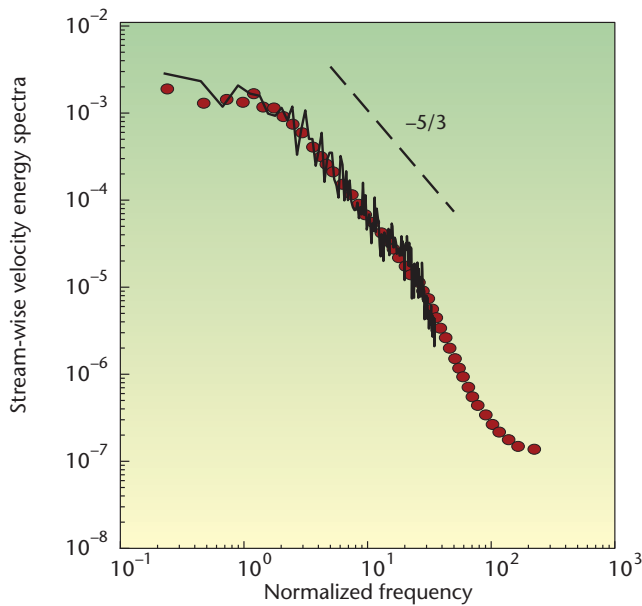


Figure 7. Stream-wise velocity energy spectra as a function of dimensionless frequency at a location in the core of the tip-leakage vortex. The solid line indicates the large-eddy simulation; the red-colored circle, the experiment; and the dashed line, the  $-5/3$  slope that is characteristic of turbulent flows.

This is accompanied by counterrotating or co-rotating induced vortices, which are generated further upstream and terminated in the blade passage due to blockage by the neighboring blade. Small vortical structures abundant near the end wall downstream from the trailing edge are the tip-separation vortices. They are extremely complicated

due to interaction with the tip-leakage vortex from the neighboring blade. (Previous experiments have reported similar observations.<sup>3</sup>)

We made extensive comparisons of the flowfields between the LES solutions and experimental measurements at locations downstream of the rotor blade. For example, Figure 6 shows a comparison of the mean stream-wise velocity contours from both the LES and experiment in a  $y$ - $z$  plane roughly half-chord downstream from the trailing edge, as an observer sees it looking upstream. Vertical bundles of the mean stream-wise velocity contours are present in the wakes of the rotor blades, and the tip-leakage vortices are found near the end wall in both the simulation and the experiment. The agreement is generally good. We observed similar agreements for Reynolds stresses.

Examining the flowfield shows that the tip-leakage vortex plays a dominant role in generating turbulence and intense pressure fluctuations in the vicinity of the tip gap near the end wall. LES can correctly predict not only the time-averaged quantities but also the wave number or frequency content of the flow energy. As Figure 7 illustrates, the LES predicts the experimental energy spectrum over a wide range of frequencies without excessive numerical dissipation, which tends to damp out the higher frequency end of the spectrum. This feature is required to accurately simulate turbulent flows. (More extensive validations of the LES solutions are available elsewhere.<sup>8</sup>)

We have also collected and analyzed detailed statistics of the pressure field to draw inferences on cavitation. Figure 8 shows the contour of the time-averaged pressure and the root-mean square of pressure fluctuations in a plane parallel to the end wall inside the tip gap. The regions of negative pressure relative to the mean values coincide with regions of strong pressure fluctuations. They appear highly correlated with the vortical structures in the tip-leakage flow, particularly in the tip-leakage and tip-separation vortices.

The negative pressure regions are susceptible to cavitation. Figure 9 shows an example of cavitation inception analysis in a plane parallel to the end wall inside the tip gap using the minimum tension criterion that Daniel Joseph proposed.<sup>9</sup> This criterion is based on the fluid's normal stress and the critical vapor pressure:

$$B_{ii} = \tau_{ii} - p + p_c > 0,$$

where  $\tau_{ii}$  is the normal stress,  $p$  is local pressure, and  $p_c$  is the pressure in the cavity. For this example, we used a  $p_c$  of 0.01, assuming the cavitation number

of 0.02 based on the cascade inlet pressure. If all three components of the stress  $B_{11}$ ,  $B_{22}$ , and  $B_{33}$  are positive, a cavity will open. Figures 9a and 9b plot instantaneous and time-averaged contours of  $B = 1/3(B_{11} + B_{22} + B_{33})$ , respectively, in regions where all three components are positive. High  $B$  levels in both the instantaneous and time-averaged contours are concentrated in the tip-leakage region. In particular, the tip-leakage vortex appears as the dominant source of cavitation. The tip-separation vortex is less important even though it involves equally low pressure (see Figure 8). This is partially due to the high positive values of the normal stress  $\tau_{ii}$  in addition to the strong negative pressure found in the tip-leakage vortex.

### Tip-Leakage Vortex Modification

In addition to studying the flow dynamics and cavitation mechanisms, we also used LES to explore ways to modify the vortex structures to minimize cavitation-associated detrimental effects. We did this by varying the tip-gap size and modifying the end-wall geometry.

### Tip-Gap Size Effect

The tip-gap size relative to the chord is a key parameter for this flow. To evaluate its effect on the vortical structures and low-pressure characteristics, we carried out two additional simulations with tip-gap sizes one-half and twice the value in the baseline case we discussed earlier.

Figure 10 shows the instantaneous isosurfaces of negative pressure (blue-colored structure) and streamtraces (colored lines) for the three different tip-gap sizes. Relative to the base tip-gap size (Figure 10b), the increased tip gap enhances both the size and strength of the tip-leakage vortex, thereby resulting in larger and more negative pressure regions along the tip-leakage vortex (Figure 10a). In contrast, as Figure 10c shows, the smaller tip gap reduces the tip-leakage vortex size and the size of the negative pressure region.

These results suggest that the smaller tip-gap size is better for minimizing the tip-leakage vortex and resulting cavitation. In addition, we observed significant differences in the generation and evolution of the tip-leakage, tip-separation, and induced vortices when using different tip-gap sizes.

### End-Wall Grooves

As we previously indicated, the tip-leakage vortex is highly correlated with the turbulent fluctuations and low-pressure regions responsible for cavitation. Therefore, a control strategy for suppressing the tip-leakage vortex is expected to also reduce or

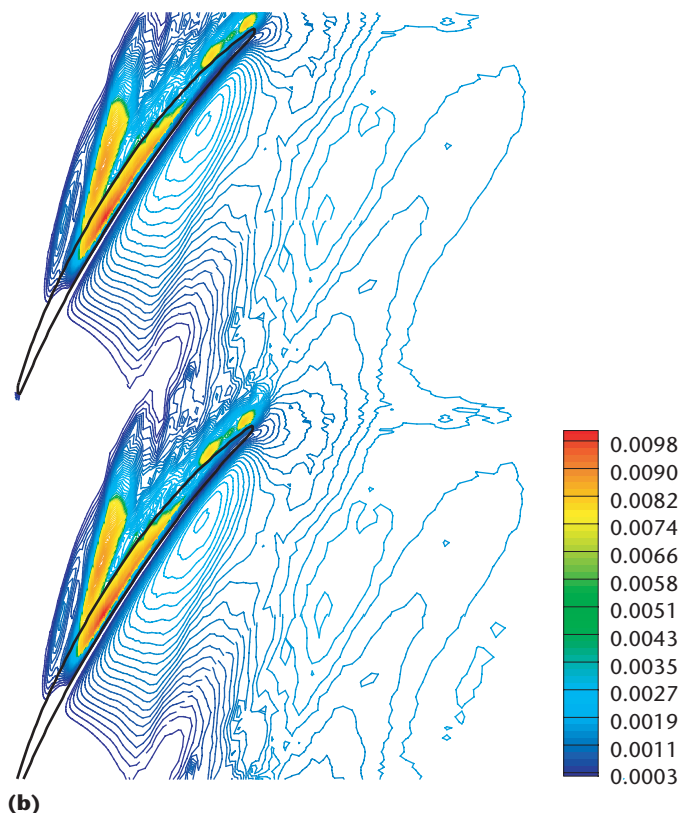
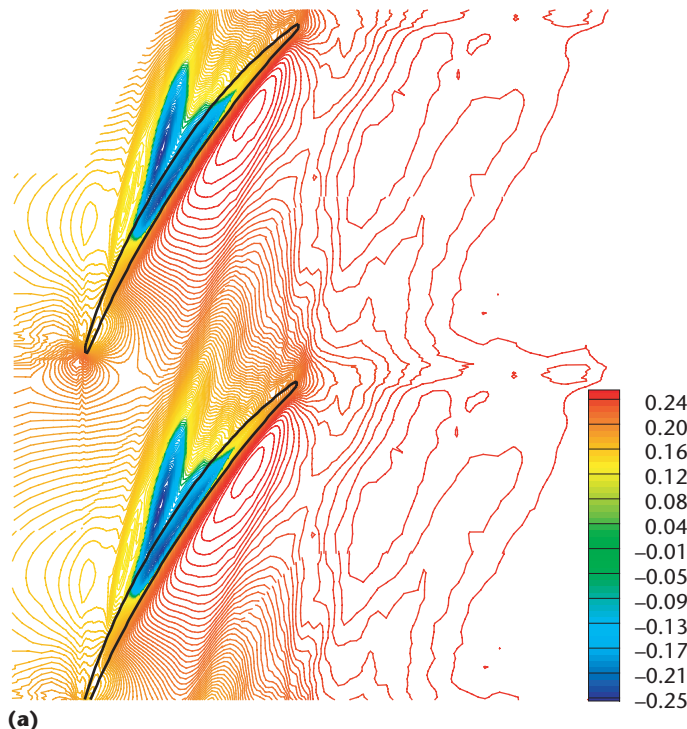


Figure 8. Pressure in the tip gap. The contours of (a) time-averaged pressure and (b) root-mean square pressure fluctuation in a plane inside the tip gap at  $z/C = 0.001$ .

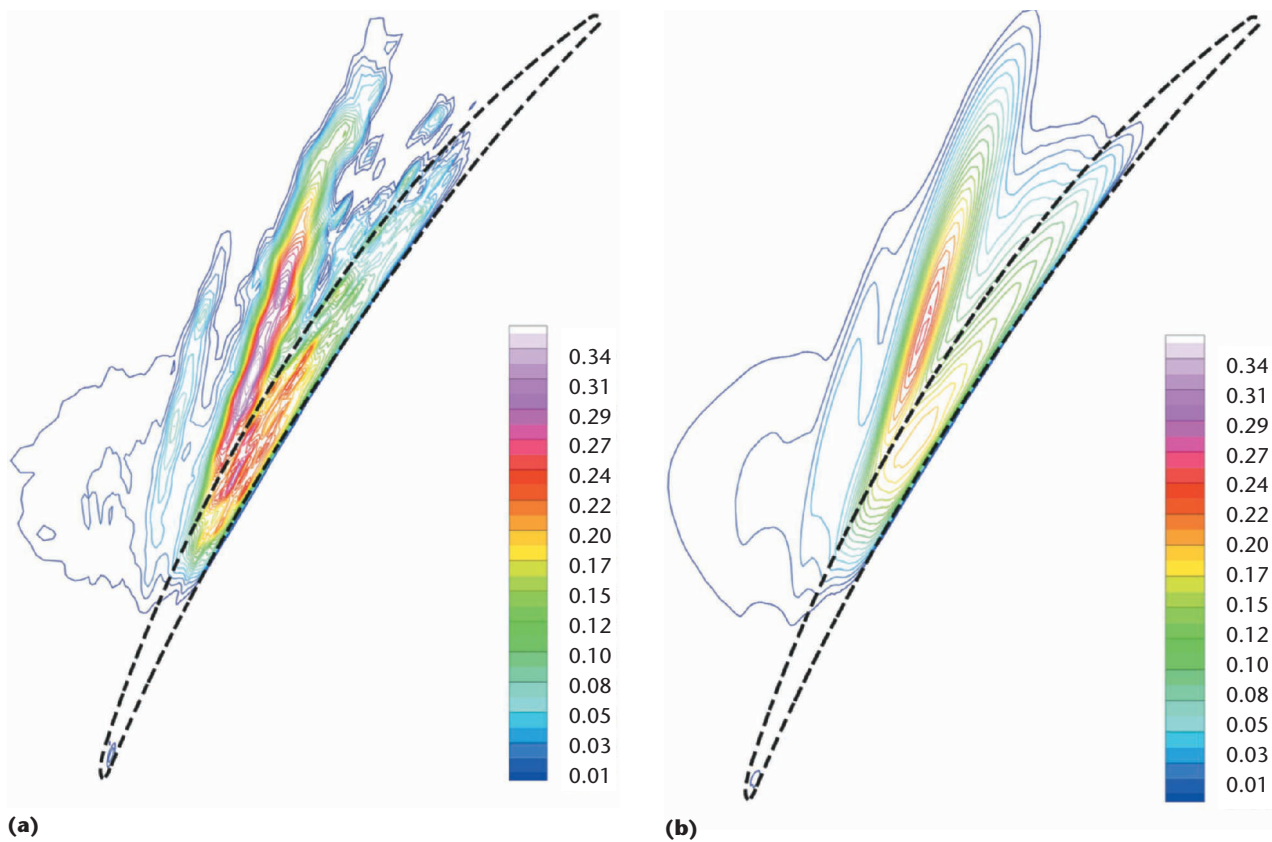


Figure 9. Cavitation criterion. The contours of (a) instantaneous and (b) time-averaged cavitation criterion,  $B = 1/3(B_{11} + B_{22} + B_{33})$ , in a plane inside the tip gap at  $z/C = 0.01$ .

eliminate cavitation and the associated unfavorable effects. Casing-wall modification has been one of the common methods for controlling tip-leakage flow. For example, Jinwoo Bae and his colleagues<sup>10</sup> devised synthetic jet actuators mounted on the casing end wall, and Donald Thompson and his colleagues<sup>11</sup> used grooved casing walls in their experimental study. As an initial attempt, we investigated the effect of an end-wall groove, shown schematically in Figure 11, using LES. The groove's location and size are determined using the information obtained from LES with the untreated end wall, and they can be optimized iteratively. The groove introduces disturbances in the tip-gap region, which interacts with the tip-leakage flow, causing enhanced mixing and less coherent flow structures.

Before applying this control strategy to the full Reynolds number (400,000) case, we assessed its feasibility and efficiency at a reduced Reynolds number of 10,000 with uniform inflow. These simplifications are partly justified by observing that the tip-leakage vortex in the tip-gap region is highly coherent and relatively insensitive to the Reynolds number. The simulation setup is the same as in the uncontrolled

baseline case, except that we used a stationary end wall and a smaller mesh with 9.5 million grid points. The end-wall groove is placed near the leading edge (approximately 10 percent of the axial chord), which corresponds to the origin of the tip-leakage vortex. The groove's depth is the same as the tip-gap size, and its width is three times the tip-gap size.


Figure 12 shows results from the simulations of controlled and uncontrolled tip-leakage flows in terms of an isosurface of the instantaneous vorticity magnitude that represents the vortex's strength. These results appear promising in the sense that the tip-leakage vortex loses its coherence more rapidly in the grooved case compared to the ungrooved one. Figure 13 provides a more quantitative comparison, showing that the velocity deficit, also reflective of the tip-leakage vortex's strength, is reduced by using the end-wall groove. This also leads to an improved downstream pressure rise because of the diminished tip-leakage vortex and its blockage effect in the cascade passage.

Using an end-wall groove can have adverse effects on performance in terms of drag, acoustics, and vibration. However, these effects can be miti-

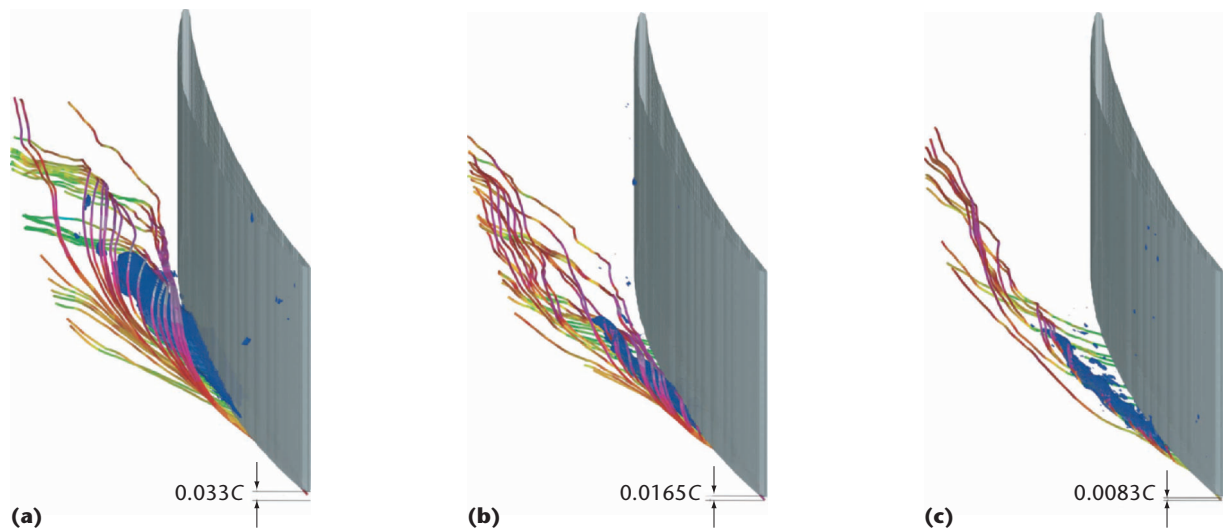


**Figure 10. Tip-gap size effect.** Snapshots of negative pressure (blue) and stream traces (colored lines) show the swirling tip-leakage flow and vortex for three different tip-gap sizes. (a) Tip gap = 0.033 chord, (b) tip gap = 0.0165 chord, and (c) tip gap = 0.0083 chord.

gated by choosing an appropriate combination of groove parameters and tip-gap size. To address these issues thoroughly, we can treat the problem in a constrained optimization framework.

**A**ided by powerful parallel computers, LES has let us examine the technologically important tip-clearance flow in unprecedented detail. Although this work does not directly simulate cavitation, we have gained new physical insights about the complex vortex structures, dynamics, and associated low-pressure events that lead to cavitation. An extension of the current methodology to multiphase flows will be useful and can potentially lead to drastic improvements in cavitation prediction. 

### Acknowledgments

We acknowledge the support of the Office of Naval Research under grant number N00014-99-1-0389, with Ki-Han Kim as program manager. Computer time was provided by the Challenge Project Grant C82 from the US Department of Defense High-Performance Computing Modernization Program (HPCMP) through Army Research Laboratory (ARL) and Aeronautical Systems Center (ASC) Major Shared Resource Centers (MSRC).

### References

1. B. Lakshminarayana, *Fluid Dynamics and Heat Transfer of Turbomachinery*, John Wiley & Sons, 1996.
2. R.T. Knapp, J.W. Daily, and F.G. Hammit, *Cavitation*, McGraw-

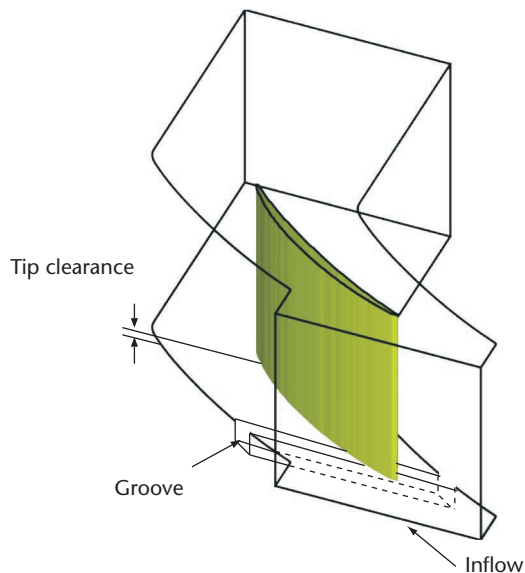


**Figure 11. Tip-clearance flow configuration with an end-wall groove.** The groove is used to weaken the tip-leakage vortex and its detrimental effects.

Hill, 1970.

3. Y. Wang, *Tip Leakage Flow Downstream of a Compressor Cascade with Moving End Wall*, master's thesis, Dept. of Aerospace Eng., Virginia Polytechnic Inst. and State Univ., 2000.
4. C. Meneveau, T.S. Lund, and W.H. Cabot, "A Lagrangian Dynamic Subgrid-Scale Model of Turbulence," *J. Fluid Mechanics*, vol. 319, 1996, pp. 233–242.
5. E.A. Fadlun et al., "Combined Immersed-Boundary Finite-Difference Methods for Three-Dimensional Complex Flow Simulations," *J. Computational Physics*, vol. 161, no. 1, 2000, pp. 35–60.



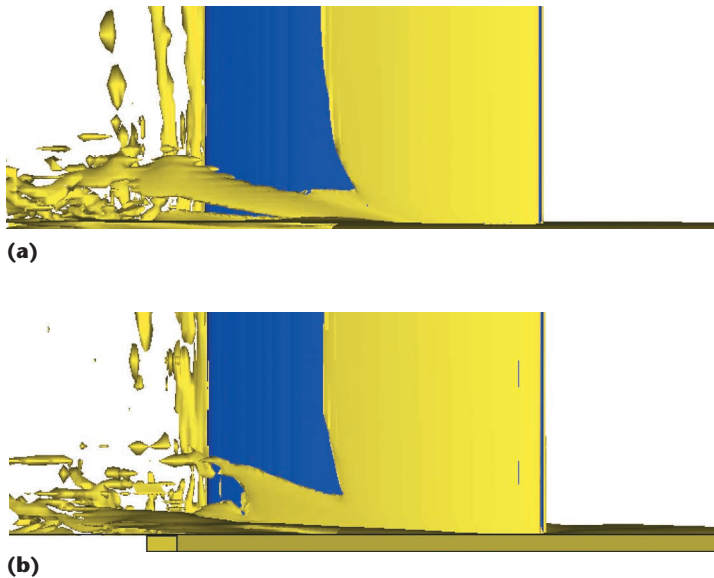


Figure 12. Effect of end-wall groove on tip-leakage vortex. Snapshots of tip-leakage vortex as represented by an isosurface of vorticity magnitude from simulations (a) without and (b) with an end-wall groove.

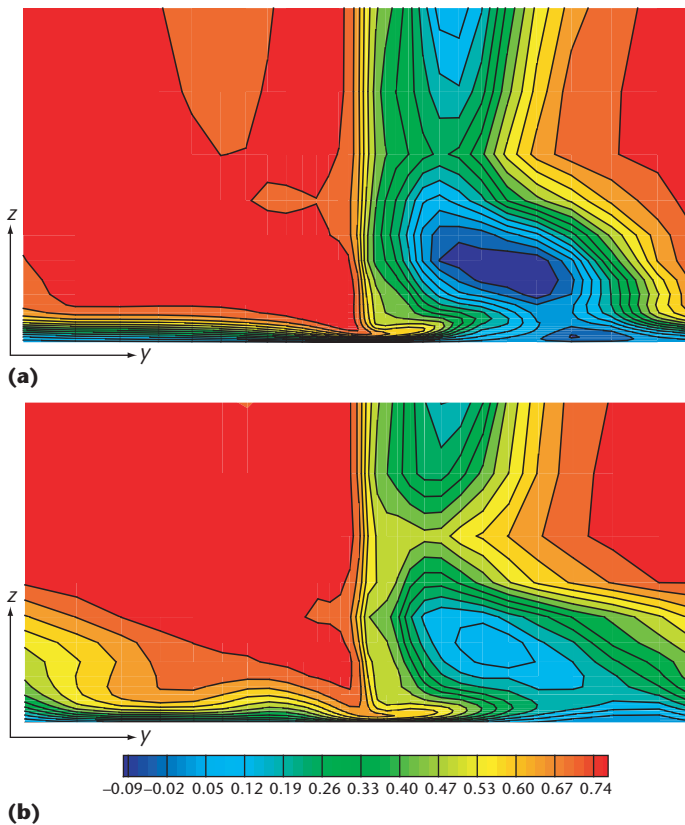


Figure 13. Effect of end-wall groove on velocity field. Contours of mean pitch-wise velocity in a plane at  $x/C = 0.6$  (a) without and (b) with end-wall groove.

6. J. Zhang, "Multigrid Method and Fourth Order Compact Difference Scheme for 2D Poisson Equation with Unequal Meshsize Discretization," *J. Computational Physics*, vol. 179, no. 1, 2002, pp. 170–179.
7. J. Jeong and F. Hussain, "On the Identification of a Vortex," *J. Fluid Mechanics*, vol. 285, 1995, pp. 69–94.
8. D. You et al., "Computational Methodology for Large-Eddy Simulation of Tip-Clearance Flows," *AIAA J.*, vol. 42, no. 2, 2004, pp. 271–279.
9. D.D. Joseph, "Cavitation and the State of Stress in a Flowing Liquid," *J. Fluid Mechanics*, vol. 366, 1998, pp. 367–378.
10. J. Bae, K.S. Breuer, and C.S. Tan, *Control of Tip Clearance Flows in Axial Compressors*, AIAA Paper 2000-2233, Fluids 2000 Conf., 2000.
11. D.W. Thompson, P.I. King, and D.C. Rabe, "Experimental Investigation of Stepped Tip Gap Effects on the Performance of a Transonic Axial-Flow Compressor Rotor," *J. Turbomachinery*, vol. 120, no. 3, 1998, pp. 477–486.

**Donghyun You** is a postdoctoral research fellow at the Center for Turbulence Research, Stanford University. His interests are in numerical simulation of complex flows and high-performance computing. He has a PhD in mechanical engineering from Stanford University. He is a member of the APS, AIAA, and ASME. Contact him at [dyou@stanford.edu](mailto:dyou@stanford.edu).

**Meng Wang** is a senior research scientist at Stanford University, working at the Stanford/NASA Center for Turbulence Research. His research interests include numerical simulation, modeling, and control of turbulent flows and aeroacoustics. He has a PhD in mechanical engineering from the University of Colorado, Boulder. He is a member of the APS, Sigma Xi, and the American Geophysical Union. Contact him at [wangm@stanford.edu](mailto:wangm@stanford.edu).

**Rajat Mittal** is an associate professor in the Department of Mechanical and Aerospace Engineering at George Washington University. His interests are in computational fluid dynamics, vortex dominated flows, fluid-structure interaction, and biofluid dynamics. He has a PhD in applied mechanics from the University of Illinois at Urbana-Champaign. He is a member of AIAA, APS, and ASME. Contact him at [mittal@gwu.edu](mailto:mittal@gwu.edu).

**Parviz Moin** is the Franklin P. and Caroline M. Johnson Professor of Mechanical Engineering, director of the Center for Turbulence Research, and director of the Institute for Computational and Mathematical Engineering at Stanford University. His interests include the physics, modeling, and control of turbulent flows. He is also interested in developing efficient numerical methods for large-scale computations and parallel computing. He has a PhD in mechanical engineering from Stanford University. He is a fellow of the American Physical Society and a member of the National Academy of Engineering. Contact him at [moin@stanford.edu](mailto:moin@stanford.edu).